TÜBİTAK

Turkish Journal of Physics

http://journals.tubitak.gov.tr/physics/

Research Article

Turk J Phys
(2019) 43: 431 – 441
© TÜBİTAK
doi:10.3906/fiz-1811-10

Precise calculation of differential cross sections for the Z boson plus jets production in proton–proton collisions at a center-of-mass energy of 13 TeV

Kadir ÖCALAN*
Department of Aviation Management, Faculty of Aviation and Space Sciences, Necmettin Erbakan University, Konya, Turkey

Received: 10.11.2018 • **Accepted/Published Online:** 29.07.2019 • **Final Version:** 21.10.2019

Abstract: The differential cross section predictions for the associated production of a Z boson and jets are presented in proton–proton collisions at a center-of-mass energy of 13 TeV. The differential cross sections are calculated by using a computational framework for the dielectron decay mode of the Z boson. Higher-order differential cross section predictions are obtained in the fiducial phase space and are compared at next-to-leading order (NLO) and next-to-NLO (NNLO) in perturbative quantum chromodynamics (pQCD). The predicted results are reported as functions of the variables including the jet multiplicity, the invariant mass of the Z boson, and transverse momenta of the Z boson and of the decay products. The predicted results are also reported for the angular correlation variables for the final state decay products. The differential results are generally improved in precision upon inclusion of the NNLO corrections. The total cross sections are calculated in the fiducial phase space at different orders in pQCD up to NNLO. The total production rates are predicted more accurately by the NNLO calculation.

Key words: Quantum chromodynamics, Z+jets, NLO and NNLO differential cross section calculations, q_T subtraction formalism

1. Introduction

The production of a vector boson in association with jets at hadron colliders provides fundamental tests for quantum chromodynamics (QCD) sector of the standard model (SM). The productions of a weak vector boson (either a W boson or a Z boson) in leptonic final states with associated jets have sufficiently large production rates and clean experimental signatures in proton–proton (pp) collisions at the CERN Large Hadron Collider (LHC). Such production processes become more important to exploit physics potential of the LHC experiments with the accumulation of more pp collision data at higher center-of-mass energies. Particularly, the production of a Z boson in dilepton decay channels along with energetic jets (Z+jets) has several outstanding aspects for high-energy physics phenomenology. The Z+jets production serves as an important experimental benchmark for detector calibration by means of jet energy scale and resolution studies. The Z+jets process can provide significant inputs for determination of parton distribution functions (PDFs) such as for constraining gluon PDF in the proton. It is not only a prominent process as a signal but also as a leading background for a number of SM processes such as single top quark, top pair, and Higgs boson productions as well as vector boson fusion and WW scattering. It is an important background to signatures of both supersymmetric and dark matter particle production in new physics searches. Its leptonic decay modes provide a strong rejection of backgrounds

*Correspondence: kadir.ocalan@konya.edu.tr

This work is licensed under a Creative Commons Attribution 4.0 International License.

in the measurements of SM processes and new physics searches. In all these aspects, a precise understanding of this process is crucial with lower theoretical uncertainty for an accurate description of experimental data of the LHC.

From an experimental point of view, the Z+jets process has been characterized by the measurements of differential cross sections at hadron colliders. Its differential cross sections have been measured as functions of various relevant kinematic and angular variables by achieving the highest possible precision. The variables are reconstructed using the Z boson and its leptonic decay products as well as the associated hadronic jets. Differential Z+jets cross sections have been previously measured in proton–antiproton collisions at a center-of-mass energy of 1.96 TeV by the CDF and D0 Collaborations at the Tevatron [1, 2]. The Z+jets production cross sections have also been measured differentially by the ATLAS, CMS, and LHCb Collaborations in pp collisions at center-of-mass energies of 7 [3–6], 8 [7–9], and 13 [10, 11] TeV at the LHC. In all of these complementary measurements, experimental data have been compared with predictions from various Monte Carlo (MC) event generators and higher-order perturbative QCD (pQCD) calculations including either next-to-leading order (NLO) or next-to-NLO (NNLO) corrections.

The need for precise prediction of the Z+jets process becomes critical for the physics motivations including accurate description of experimental data. Properties of this process including its production cross sections are required to be predicted by theoretical calculations in higher-order pQCD. The higher-order theoretical calculations including NLO and NNLO corrections in pQCD are needed to be performed for improving the accuracy in description of large experimental data accumulated by the LHC experiments. In the precise predictions of the SM processes comprising the Z+jets production, QCD radiative corrections are required to be included in the higher-order computations. The field of NNLO QCD computations has been rapidly developing to provide fully differential calculations for various hadron collider processes. NNLO differential calculations have been available for quite some time for Z+1-jet [12, 13] production. Despite the significant progress, publicly available NNLO computations employ a limited set of methods for the evaluation of divergencies in their differential cross section calculations. Moreover, available NNLO programs typically perform differential computations for a few specific processes such as FEWZ [14] and DYNNLO [15].

In this paper, differential cross section predictions at NLO and NNLO accuracies for the Z+jets production in the dielectron decay channel are presented based on pp collisions at a center-of-mass energy of 13 TeV. The differential cross sections are calculated in the fiducial phase space, where a Z boson is defined as a pair of oppositely charged electrons with invariant mass in the range 91 ± 20 GeV. The differential results are presented for the variables including the jet multiplicity, the invariant mass of the Z boson, and transverse momenta of the Z boson and of the decay products as well as the angular correlation variables for the final state products. Total fiducial cross section predictions are also presented at different orders in pQCD. The higher-order differential and total cross sections are predicted by employing the computational framework *MATRIX* [15, 16] in which the q_T-subtraction method [17, 18] is used.

2. (N)NLO computational setup

The computation of a QCD cross section at NLO requires the evaluation of real emission corrections from tree-level processes with one additional parton and virtual corrections from one-loop scattering amplitudes. In the NNLO cross section computation, real emission corrections from one-loop scattering amplitudes with one additional parton, real emission corrections from tree-level processes with up to two additional partons, and virtual corrections from two-loop scattering amplitudes are required to be evaluated properly. The evaluation of both real emission and virtual corrections in a fully differential cross section computation at (N)NLO is a

nontrivial task due to the presence of infrared (IR) divergences at the intermediate stages of the calculation. A straightforward combination of contributions from real and virtual corrections is not possible as divergences affect real and virtual components in different ways. Various methods have been proposed and used to provide resolution for these issues [19–23]. In the present study, the (N)NLO computation in *MATRIX* [15, 16] is achieved by using a process-independent implementation of the transverse momentum q_T-subtraction method [17, 18] for the cancellation of divergences in the calculations of the cross sections. The *OPENLOOPS* MC program [24–26] is integrated with *MATRIX* (N)NLO computation to acquire all tree-level and one-loop scattering amplitudes. In the q_T-subtraction method, where q_T refers to transverse momentum of colorless system (i.e. a system of particles without QCD interactions), the behavior of the q_T distribution at small values is explicitly known up to NNLO by means of the q_T resummation formalism [27, 28]. The q_T resummation formalism provides sufficient information to construct process-independent IR subtraction counterterm for the calculation of cross sections which is also applicable for several processes including the Z+jets production. The differential cross section in the q_T-subtraction approach $d\sigma$ for a process $pp \to F + X$ (where F is a colorless system) can be written at (N)NLO as

$$d\sigma^{F}_{(N)NLO} = [d\sigma^{F+jet}_{(N)LO} - d\sigma^{CT}_{(N)LO}] + H^{F}_{(N)NLO} \otimes d\sigma^{F}_{LO}. \tag{2.1}$$

In the square bracket of Eq. 2.1, $d\sigma^{F+jet}_{(N)LO}$ term represents the cross section for the system $F + jet$ at (N)LO, while the process-independent counterterm $d\sigma^{CT}_{(N)LO}$ guarantees the cancellation of the $F + jet$ cross section divergence at (N)LO. The square bracket is IR finite in the limit $q_T \to 0$, but the terms $d\sigma^{F+jet}_{(N)LO}$ and $d\sigma^{CT}_{(N)LO}$ are separately divergent. In Eq. 2.1, the $H^{F}_{(N)NLO}$ term is the hard-collinear function at (N)NLO and the $d\sigma^{F}_{LO}$ term is the LO cross section of the system F. The hard-collinear function H^{F} has been explicitly computed up to NNLO for vector boson production [18]. In the (N)NLO computations of the q_T-subtraction formalism, a residual dependence parameter $r = q_T/m$ is employed, where m is the invariant mass of the colorless system. This residual dependence comes from power-suppressed terms that remain after the subtraction of the IR singular contribution at finite values and vanish only in the limit $q_T \to 0$. In the next step, a cut-off value for this residual dependence r_{cut} is introduced to render both terms $d\sigma^{F+jet}_{(N)LO}$ and $d\sigma^{CT}_{(N)LO}$ separately finite. In the differential cross section calculations of this paper at (N)NLO, $r_{cut} = 0.0015$ (0.15%) is used and below this cut $d\sigma^{F+jet}_{(N)LO}$ and $d\sigma^{CT}_{(N)LO}$ terms are assumed to be identical up to power-suppressed contributions. The total cross sections in this paper are reported for both $r_{cut} = 0.15\%$ and for the extrapolation in the limit $r_{cut} \to 0$.

The cross section computation of the Z+jets production is configured for pp collisions at the LHC using a center-of-mass energy of 13 TeV. The Z+jets process in the dielectron decay channel $pp \to Z \to e^+e^- + X$, where the Z boson is off-shell, is set up with the *MATRIX* framework. The final state X refers to any other final state including at most one (two) additional parton(s) in the (N)NLO computation. The renormalization and factorization scales are both chosen to be the Z boson mass $\mu_R = \mu_F = m(Z) = 91.1876$ GeV in the (N)NLO cross section computations. The scales are used in the estimation of uncertainties from missing higher-order contributions by independently varying the μ_R and μ_F by a factor of 0.5 and 2. All possible combinations are taken into account in the variations except the cases where one scale is varied by a factor of 0.5 and the other one by a factor of 2 at the same time.

The *LHAPDF 6.2.0* [29] is used for the evaluation of PDFs from data files in the computations. The PDF sets *NNPDF31_lo_as_0118*, *NNPDF31_nlo_as_0118*, and *NNPDF31_nnlo_as_0118* are used from the NNPDF Collaboration [30] for the LO, NLO, and NNLO cross section calculations, respectively. The PDF sets are all based on a constant strong coupling $\alpha_s(m(Z)) = 0.118$ assuming an electroweak scale fixed at the Z boson mass $m(Z)$=91.1876 GeV.

3. Fiducial phase space

In the differential and total cross section calculations of this paper realistic fiducial selection cuts are imposed. The fiducial cuts are selected to match with the ones that are used in the latest measurements of the LHC experiments. The Z boson in the decay chain of pp$\rightarrow$Z$\rightarrow e^+e^-$+jets is defined as a pair of an electron and an antielectron (positron) in the dielectron invariant mass window of 91 $\pm$ 20 GeV. This dielectron invariant mass requirement was used in the most recent experimental measurements by the ATLAS [10] and CMS [11] Collaborations to enhance signal sensitivity of the Z boson production. Either an electron or a positron is required to have transverse momentum $p_T > 20$ GeV in the absolute pseudorapidity $|\eta|$ acceptance of 2.4. The jets are clustered using the anti-k_T algorithm [31] with the distance parameter ΔR=0.4, where ΔR is defined using the separation in jet η and in jet azimuthal angle ϕ as $\Delta R = \sqrt{\Delta\eta^2 + \Delta\phi^2}$. The fiducial selection of the jets include $p_T > 30$ GeV requirement in the absolute rapidity $|y|$ acceptance of 2.4. The jets are selected to refer to all parton-level jets; gluons and 5 light quarks including a massless bottom quark b such as from the gluon splitting process $g \rightarrow b\bar{b}$, which is essentially needed to keep jet observables IR safe. The fiducial selection criteria are given in Table 1.

Table 1. The fiducial selection cuts that are imposed for the differential and total cross section calculations of the $Z \rightarrow e^+e^- + X$ process.

Fiducial cuts	jet	lepton	dilepton invariant mass
$(Z \rightarrow e^+e^- + X)$	$p_T(jet) > 30$ GeV $\|y(jet)\| < 2.4$	$p_T(e^{\pm}) > 20$ GeV $\|\eta(e^{\pm})\| < 2.4$	71 GeV$\leq m_{e^+e^-} \leq$111 GeV

4. Phenomenological results

In this section, differential cross section predictions for the Z+jets production in the dielectron decay mode are presented in the fiducial phase space (as summarized in Table 1). The total fiducial cross section predictions for the Z+jets production in the dielectron decay mode are also given at the end of this section. The central results of the cross sections along with the lower and upper scale uncertainties are given for each variable under study. The differential results are presented at both NLO and NNLO accuracies, while the total cross sections are presented at LO, NLO, and NNLO accuracies.

The differential cross sections are calculated as a function of the jet multiplicity N_{jets} for the Z+jets production. The differential results are calculated up to one jet at NLO and up to two jets at NNLO which are given in Table 2. The scale uncertainties are down to 2% level at NNLO for the Z+1-jet production. The predicted differential cross sections as functions of the jet multiplicities in Table 2 are quite consistent within the uncertainties with the recent ATLAS [10] and CMS [11] results including both data measurements and MC predictions from various event generators. The differential cross sections at (N)NLO are calculated for the invariant mass of the Z boson m_Z in the dielectron invariant mass window of $71 \leq m_{e^+e^-} \leq 111$ GeV and are

given in Table 3. The NLO and NNLO differential cross sections are consistent within uncertainties for the m_Z range of 90–95 GeV, where the measured Z boson mass $m(Z)$=91.1876 GeV falls in. In this invariant mass range of the measured $m(Z)$, the scale uncertainties are reduced to less than 1% at NNLO accuracy.

Table 2. The differential cross sections as a function of N_{jets} for the $Z \to e^+e^- + X$ process calculated up to one (two) jet(s) at (N)NLO. The up and down scale uncertainties due to the variations in μ_R and μ_F are quoted in percent in addition to the central values.

N_{jets}	$\mathrm{d}\sigma_{NLO}/\mathrm{dN}_{jets}$ $(Z \to e^+e^- + X)$	$\mathrm{d}\sigma_{NNLO}/\mathrm{dN}_{jets}$ $(Z \to e^+e^- + X)$
1	$100.77^{+11.7\%}_{-9.4\%}$ pb	$108.57^{+2.1\%}_{-2.4\%}$ pb
2	–	$29.86^{+24.8\%}_{-18.0\%}$ pb

Table 3. The differential cross sections in bins of m_Z for the $Z \to e^+e^- + X$ process calculated at NLO and NNLO. The results are presented for the m_Z ranges in the dielectron invariant mass range of 71–111 GeV. The up and down scale uncertainties due to the variations in μ_R and μ_F are quoted in percent in addition to the central values.

m_Z (GeV)	$\mathrm{d}\sigma_{NLO}/\mathrm{d}m_Z$ $(Z \to e^+e^- + X)$	$\mathrm{d}\sigma_{NNLO}/\mathrm{d}m_Z$ $(Z \to e^+e^- + X)$
71–75	$1.03^{+2.8\%}_{-2.9\%}$ pb	$1.40^{+5.5\%}_{-3.9\%}$ pb
75–80	$2.18^{+2.9\%}_{-4.6\%}$ pb	$2.22^{+0.2\%}_{-0.9\%}$ pb
80–85	$4.94^{+2.9\%}_{-4.8\%}$ pb	$5.28^{+1.2\%}_{-2.1\%}$ pb
85–90	$31.72^{+2.5\%}_{-4.2\%}$ pb	$33.75^{+0.7\%}_{-0.9\%}$ pb
90–95	$104.93^{+2.6\%}_{-4.6\%}$ pb	$105.03^{+0.7\%}_{-0.7\%}$ pb
95–100	$8.88^{+2.6\%}_{-4.1\%}$ pb	$9.06^{+1.1\%}_{-1.5\%}$ pb
100–105	$2.50^{+1.7\%}_{-3.3\%}$ pb	$3.04^{+2.5\%}_{-2.0\%}$ pb
105–111	$1.62^{+4.1\%}_{-5.4\%}$ pb	$1.50^{+5.6\%}_{-8.9\%}$ pb

The differential cross section distributions at NLO and NNLO are predicted and are overlaid in the same plot in comparisons of a given variable spectrum. The theoretical uncertainties due to the variations in μ_R and μ_F scales are shown in hatched bands around central points in each differential distribution. In the lower panels of each plot, ratios of NNLO differential cross section to NLO differential cross section are shown with lower and higher scale uncertainties of ratios. The p_T is an important variable having sensitivity to higher-order corrections in cross section calculations and can be used to probe hard scattering dynamics of the Z+jets production. The differential cross section as a function of the Z boson p_T $p_T(Z)$ is predicted at NLO and NNLO. The $p_T(Z)$ distributions can provide an important constraint on the gluon PDF [32]. The NLO and NNLO differential distribution shapes are consistent for the $p_T(Z)$ variable as given in Figure 1 (left). The differential cross section predictions as a function of the first energetic (leading) jet p_T $p_T(j_1)$ are given in Figure 1 (right). The differential distribution shapes are consistent in the low and intermediate regions of the $p_T(j_1)$ variable. The NNLO prediction is higher in the higher ranges of the $p_T(j_1)$ variable than the NLO one. The scales uncertainties increase towards the higher ranges of the $p_T(Z)$ and $p_T(j_1)$ variables. The differential cross sections are calculated as functions of the electron and positron p_T variables $p_T(e^-)$ and $p_T(e^+)$ which are shown in Figure 2. The $p_T(e^-)$ and $p_T(e^+)$ shapes of the differential distributions are overall consistent at NLO and NNLO, while the NNLO calculation predicts slightly higher differential cross sections for the entire ranges. In all the differential p_T predictions, the precision achieved by the NNLO calculations is comparable to

or higher than NLO results. In the NNLO-to-NLO differential cross section ratios for the $p_T(Z)$, $p_T(e^-)$, and $p_T(e^+)$ variables, the ratios are consistently around the band of 1.4–1.6 within uncertainties. The NNLO-to-NLO ratios for the $p_T(j_1)$ variable increase up to ∼9.6 within uncertainties with the increasing $p_T(j_1)$, such that the included NNLO corrections becomes larger for higher values of the leading jet p_T.

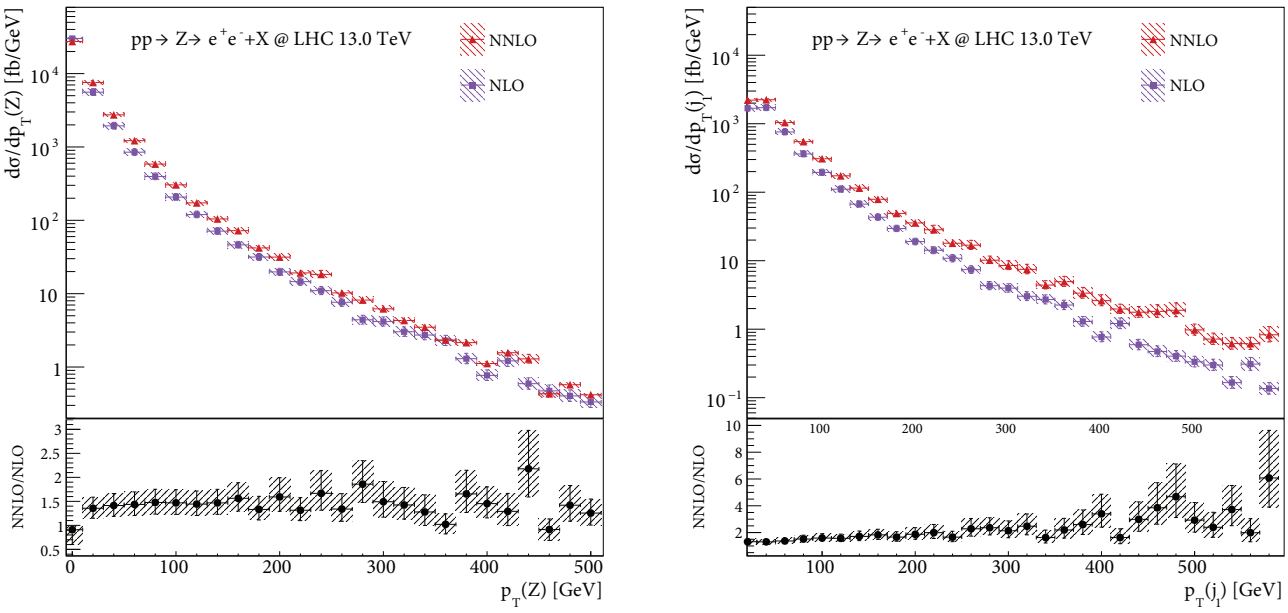

Figure 1. The differential cross sections as functions of the $p_T(Z)$ (left) and $p_T(j_1)$ (right) for the $Z \to e^+e^- + X$ process predicted at NLO and NNLO. The results are presented for the $p_T(Z)$ range of 0–500 GeV and $p_T(j_1)$ range of 0–600 GeV. The scale uncertainties due to the variations in μ_R and μ_F are included in colored hatched bands around central points. In the lower panels, ratios of differential cross sections $\mathrm{d}\sigma_{NNLO}/\mathrm{d}\sigma_{NLO}$ are given with upper and lower uncertainties due to variations of corresponding cross sections by scale uncertainties.

The differential results are also calculated for the angular correlation variables in the fiducial phase space of the Z+jets production. The differential cross sections are predicted for the azimuthal separation $\Delta\phi(e^+, e^-)$ and the angular distance $\Delta R(e^+, e^-)$ between the directions of the outgoing positron and electron, where the ΔR is defined in terms of separation in y-ϕ plane as $\Delta R = \sqrt{\Delta y^2 + \Delta\phi^2}$. The differential cross section distributions increase with the increasing $\Delta\phi(e^+, e^-)$ values up to ∼3.1 as shown in Figure 3 (left) indicating a tendency for back-to-back azimuthal separation predicted by the calculations. The differential distributions are shown in Figure 3 (right) for the $\Delta R(e^+, e^-)$ variable, where both NLO and NNLO calculations predict a clear peak around 3.2. In both the $\Delta\phi(e^+, e^-)$ and $\Delta R(e^+, e^-)$ calculations, NNLO-to-NLO cross section ratios are generally around the band of 1.4–1.6 within uncertainties over almost the entire ranges of these variables. Additionally, the differential cross section is also calculated for the angular distance between the leading jet and the hardest lepton $\Delta R(j_1, l_1)$ where the lepton is inclusive in flavor (it could be either an electron or a muon). The differential cross sections as a function of the $\Delta R(j_1, l_1)$ variable is calculated for the central ranges of 2.0–4.0 to probe highest precision that could be achieved by employing the NNLO calculations. The differential results as a function of the $\Delta R(j_1, l_1)$ variable are summarized in Table 4. The estimated theoretical uncertainties are in the range of 1.7%–16.1% in this NNLO calculation.

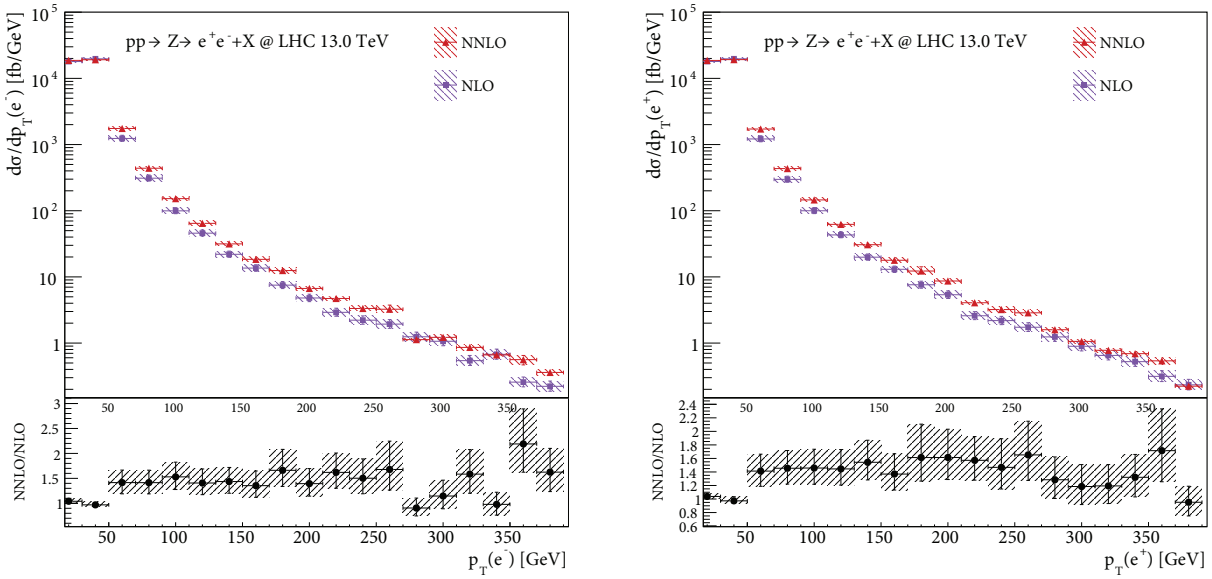

Figure 2. The differential cross sections as functions of the $p_T(e^-)$ (left) and $p_T(e^+)$ (right) for the $Z \to e^+e^- + X$ process predicted at NLO and NNLO. The results are presented for the p_T range of 0–390 GeV. The scale uncertainties due to the variations in μ_R and μ_F are included in colored hatched bands around central points. In the lower panels, ratios of differential cross sections $\mathrm{d}\sigma_{NNLO}/\mathrm{d}\sigma_{NLO}$ are given with upper and lower uncertainties due to variations of corresponding cross sections by scale uncertainties.

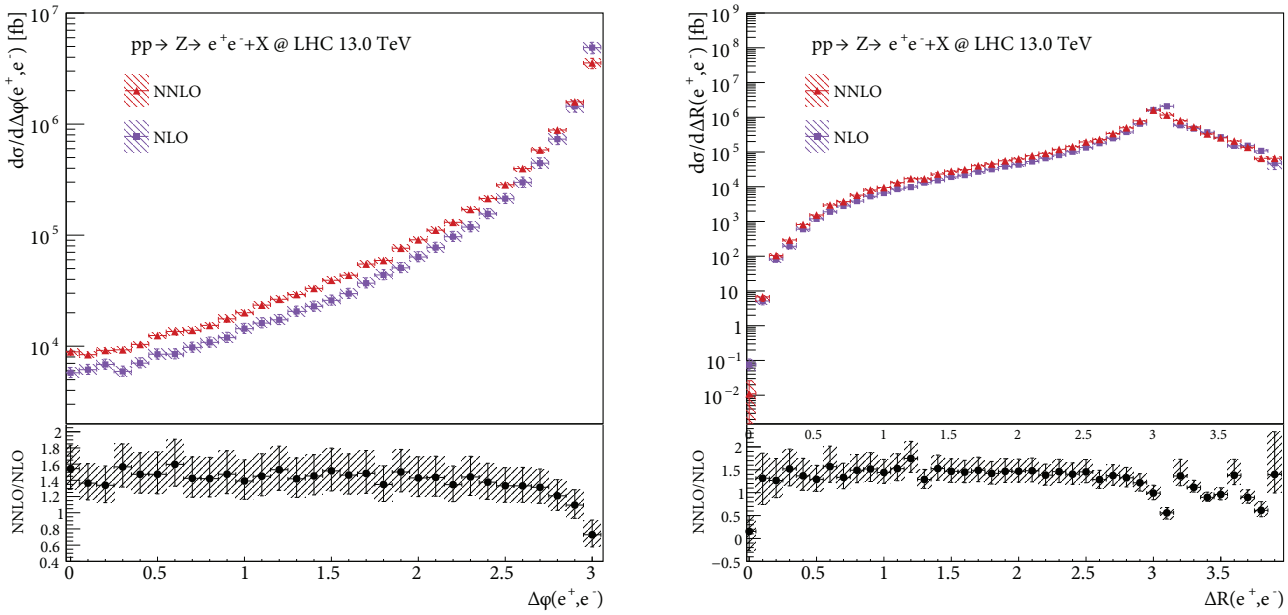

Figure 3. The differential cross sections as functions of the $\Delta\phi(e^+, e^-)$ (left) and $\Delta R(e^+, e^-)$ (right) for the $Z \to e^+e^- + X$ process predicted at NLO and NNLO. The results are presented for the $\Delta\phi(e^+, e^-)$ range of 0–3.1 rad and $\Delta R(e^+, e^-)$ range of 0–4.0 rad. The scale uncertainties due to the variations in μ_R and μ_F are included in colored hatched bands around central points. In the lower panels, ratios of differential cross sections $\mathrm{d}\sigma_{NNLO}/\mathrm{d}\sigma_{NLO}$ are given with upper and lower uncertainties due to variations of corresponding cross sections by scale uncertainties.

Table 4. The differential cross sections in bins of $\Delta R(j_1, l_1)$ for the $Z \to l^+l^- + X$ process calculated at NNLO. The results are presented for the $\Delta R(j_1, l_1)$ variable using the central regions of 2.0–4.0 rad. The up and down scale uncertainties due to the variations in μ_R and μ_F are quoted in percent in addition to the central values.

$\Delta R(j_1, l_1)$	$d\sigma_{NNLO}/\Delta R(j_1, l_1)$ $(Z \to l^+l^- + X)$	$\Delta R(j_1, l_1)$	$d\sigma_{NNLO}/\Delta R(j_1, l_1)$ $(Z \to l^+l^- + X)$
2.0–2.1	$23.48^{+16.1\%}_{-12.3\%}$ pb	3.0–3.1	$129.32^{+3.3\%}_{-3.9\%}$ pb
2.1–2.2	$36.02^{+12.6\%}_{-10.0\%}$ pb	3.1–3.2	$114.93^{+5.4\%}_{-5.3\%}$ pb
2.2–2.3	$44.74^{+9.0\%}_{-7.7\%}$ pb	3.2–3.3	$74.77^{+6.4\%}_{-5.9\%}$ pb
2.3–2.4	$50.21^{+4.7\%}_{-4.8\%}$ pb	3.3–3.4	$54.21^{+6.7\%}_{-6.1\%}$ pb
2.4–2.5	$62.26^{+3.1\%}_{-3.8\%}$ pb	3.4–3.5	$35.90^{+4.7\%}_{-4.8\%}$ pb
2.5–2.6	$78.24^{+3.1\%}_{-3.8\%}$ pb	3.5–3.6	$33.17^{+8.2\%}_{-7.1\%}$ pb
2.6–2.7	$95.80^{+3.5\%}_{-3.0\%}$ pb	3.6–3.7	$23.64^{+6.9\%}_{-6.3\%}$ pb
2.7–2.8	$104.85^{+1.9\%}_{-3.0\%}$ pb	3.7–3.8	$19.90^{+8.4\%}_{-7.2\%}$ pb
2.8–2.9	$108.10^{+1.7\%}_{-1.9\%}$ pb	3.8–3.9	$19.00^{+11.0\%}_{-8.9\%}$ pb
2.9–3.0	$132.38^{+2.9\%}_{-3.7\%}$ pb	3.9–4.0	$14.21^{+11.0\%}_{-9.0\%}$ pb

The total cross sections in the fiducial phase space of the Z+jets production (Table 1) are calculated at LO, NLO, and NNLO accuracies. The results are obtained at (N)NLO using the r_{cut} by means of the q_T-subtraction method as discussed in Section 2. The (N)NLO cross sections are calculated by using a fixed cut-off value of $r_{cut} = 0.15\%$ ($\sigma^{r_{cut}}_{(N)NLO}$) and by using the extrapolation in the limit $r_{cut} \to 0$ ($\sigma^{extrapolated}_{(N)NLO}$). The corresponding up and down scale uncertainties are included for the the predictions of the total production rates in the LO, NLO, and NNLO calculations as given in Table 5. The highest cross section is predicted in the fixed r_{cut} scheme at NLO, while the scale uncertainties are comparable in both fixed r_{cut} and $r_{cut} \to 0$ schemes at NLO. In contrast to the NLO predictions, the highest total cross section is predicted in the $r_{cut} \to 0$ scheme at NNLO. The corresponding scale uncertainties at NNLO are less than the percent level in the fixed r_{cut} scheme, while they increase up to 1.5% in the $r_{cut} \to 0$ scheme. At all the orders, the most precise total cross sections results are obtained by the NNLO calculations.

The relative sizes of the higher-order corrections in terms of K factors at NLO and NNLO are also calculated from the predicted total rates in Table 5. The relative sizes of these corrections are calculated as $K_{NLO} = (\sigma_{NLO} - \sigma_{NLO})/\sigma_{LO}$ and $K_{NNLO} = (\sigma_{NNLO} - \sigma_{NLO})/\sigma_{NLO}$. K factors at NLO and NNLO are calculated using the results obtained in both the fixed $r_{cut} = 0.15\%$ and the extrapolation $r_{cut} \to 0$ schemes. The K factors, showing the sizes of the included higher-order corrections in the cross section calculations at NLO and NNLO, are reported in Table 6. The highest K factor is predicted in the fixed r_{cut} scheme at NLO while the highest K factor is predicted in the $r_{cut} \to 0$ scheme at NNLO. There are approximately up to 24% and up to 10% increases in going from LO to NLO and from NLO to NNLO cross sections, respectively.

5. Summary and conclusion

The fully differential cross section predictions for the Z+jets production in the dielectron decay channel in pp collisions at a center-of-mass energy of 13 TeV are presented. The differential cross sections are calculated in the fiducial phase space where the Z boson is defined as a pair of oppositely charged electrons with invariant mass in the range 91± 20 GeV. The differential results are reported at NLO and NNLO in pQCD by using

Table 5. The total production cross sections in the fiducial phase space for the $Z \to e^+e^- + X$ process calculated at LO, NLO, and NNLO. The (N)NLO cross sections are reported for a finite q_T-subtraction cut-off $r_{cut} = 0.15\%$ ($\sigma^{r_{cut}}_{(N)NLO}$) and for the extrapolation in the q_T-subtraction limit $r_{cut} \to 0$ ($\sigma^{extrapolated}_{(N)NLO}$). The scale uncertainties due to the variations in μ_R and μ_F are associated to the central results in percent.

Process	σ_{LO}	$\sigma^{r_{cut}}_{NLO}$	$\sigma^{extrapolated}_{NLO}$	$\sigma^{r_{cut}}_{NNLO}$	$\sigma^{extrapolated}_{NNLO}$
$Z \to e^+e^- + X$	$636.5^{+12.3\%}_{-12.8\%}$ pb	$789.0^{+2.5\%}_{-4.5\%}$ pb	$771.4^{+2.6\%}_{-4.3\%}$ pb	$806.5^{+0.5\%}_{-0.8\%}$ pb	$850.9^{+1.2\%}_{-1.5\%}$ pb

Table 6. The relative sizes of the higher-order corrections in the total NLO and NNLO cross sections by means of the K factors for the $Z \to e^+e^- + X$ process. The K factors at (N)NLO are calculated separately in the fixed $r_{cut} = 0.15\%$ and the extrapolation $r_{cut} \to 0$ schemes using the $\sigma^{r_{cut}}_{(N)NLO}$ and $\sigma^{extrapolated}_{(N)NLO}$ results.

Process	$K^{r_{cut}}_{NLO}$	$K^{extrapolated}_{NLO}$	$K^{r_{cut}}_{NNLO}$	$K^{extrapolated}_{NNLO}$
$Z \to e^+e^- + X$	+23.9%	+21.2%	+2.2%	+10.3%

the q_T-subtraction method. The (N)NLO differential results are predicted using a fixed residual dependence parameter cut $r_{cut} = 0.15\%$ in the q_T-subtraction method. The predictions are obtained at (N)NLO as functions of the several important kinematical and angular variables that are sensitive to the inclusion of higher-order corrections. Theoretical uncertainties are estimated using the variations in the μ_R and μ_F scales and are reported with the central cross section values. The *NNPDF31* PDF sets are used in the calculations that are based on a constant strong coupling $\alpha_s(m(Z)) = 0.118$. The differential cross sections are predicted as functions of the jet multiplicity N_{jets} up to one (two) jet(s) at (N)NLO and of the Z boson invariant mass m_Z. The scale uncertainties are reduced to 2% level in the NNLO prediction for the Z+1-jet production and to less than the percent level in the m_Z range of 90–95 GeV at NNLO. The differential cross sections are predicted as a function of the transverse momentum p_T variable which is highly sensitive to inclusion of higher-order corrections. They are presented for the Z boson p_T $p_T(Z)$, the leading jet p_T $p_T(j_1)$, and the electron and positron p_T $p_T(e^-)$ and $p_T(e^+)$. The NLO and NNLO differential distributions are consistent for the $p_T(Z)$, $p_T(e^-)$, and $p_T(e^+)$ variables with the exception of higher ranges of the $p_T(j_1)$ variable where the NNLO calculation predicts higher differential distribution in comparison to the NLO calculation. The (N)NLO scale uncertainties generally increase towards higher values of the p_T values. In the NNLO-to-NLO differential cross section ratios for the $p_T(Z)$, $p_T(e^-)$, and $p_T(e^+)$ variables, the ratios are overall consistent within uncertainties around the band of 1.4–1.6 over almost the entire ranges. However, the NNLO-to-NLO ratios increase up to $\sim$9.6 within uncertainties towards higher $p_T(j_1)$ values such that more corrections are included for the higher values of the $p_T(j_1)$ variable in the NNLO calculation. The differential predictions are also reported as functions of the angular correlation variables including the azimuthal separation $\Delta\phi(e^+, e^-)$ and the angular distance $\Delta R(e^+, e^-)$ between the outgoing positron and electron as well as the angular distance $\Delta R(j_1, l_1)$ between the leading jet and the hardest lepton inclusive in flavor. The angular correlation variables are sensitive to both perturbative and nonperturbative (i.e. parton showers) effects for the cross section calculations. The differential distributions consistently increase at both NLO and NNLO with the increasing values of the $\Delta\phi(e^+, e^-)$ variable up to $\sim$3.1. The electron and positron are mostly predicted to be back-to-back azimuthally. The (N)NLO differential distributions are in agreement and predict a a clear peak around 3.2 for the $\Delta R(e^+, e^-)$ variable. In both the $\Delta\phi(e^+, e^-)$ and $\Delta R(e^+, e^-)$ predictions, NNLO-to-NLO cross section ratios are generally around the

band of 1.4–1.6 within uncertainties over almost the entire ranges. The differential results are presented in the central ranges of 2.0–4.0 of the $\Delta R(j_1, l_1)$ variable, where the estimated theoretical uncertainties at NNLO are as low as 1.7%. In all the predicted differential cross sections, the precision achieved by the NNLO calculations is generally higher than or at least comparable to NLO results.

The fiducial total cross section predictions are also calculated and compared at the LO, NLO, and NNLO accuracies for the Z+jets production in the dielectron decay channel in pp collisions at 13 TeV. The total cross sections at (N)NLO are predicted using both the fixed cut $r_{cut} = 0.15\%$ and the extrapolation $r_{cut} \to 0$ schemes in the q_T-subtraction method. In the calculations of total rates, the *NNPDF31* PDF sets are used and theoretical uncertainties are reported along with the central cross section values. The highest cross section is predicted in the fixed r_{cut} scheme at NLO, whereas the highest cross section is obtained in the $r_{cut} \to 0$ scheme at NNLO. Nevertheless, the estimated scale uncertainties at NNLO are less than the percent level in the fixed r_{cut} scheme, while they increase up to 1.5% in the $r_{cut} \to 0$ scheme. At all the orders, the most precise total cross sections results are obtained upon inclusion of the NNLO corrections. The relative sizes of the higher-order corrections in terms of K factors at (N)NLO are also predicted from the total rates in both the fixed $r_{cut} = 0.15\%$ and the extrapolation $r_{cut} \to 0$ schemes. The highest K factor is predicted in the fixed r_{cut} scheme ($r_{cut} \to 0$ scheme) at (N)NLO. The predicted K factors show that there are approximately up to 24% and up to 10% increases in going from LO to NLO and from NLO to NNLO cross sections, respectively.

References

[1] Aaltonen, T.; Adelman, J. A.; Akimoto, T.; Albrow, M. G.; Gonzalez, B. A.; Amerio, S.; Amidei, D.; Anastassov, A.; Annovi, A.; Antos, J. et. al. *Phys. Rev. Lett.* **2008**, *100*, 102001.

[2] Abazov, V. M.; Abbott, B.; Abolins, M.; Acharya, B. S.; Adams, M.; Adams, T.; Aguilo, E.; Ahsan, M.; Alexeev, G. D.; Alkhazov, G. et. al. *Phys. Lett. B* **2008**, *669*, 278-286.

[3] Aad, G.; Abajyan, T.; Abbott, B.; Abdallah, J.; Khalek, S. A.; Abdelalim, A. A.; Abdinov, O.; Aben, R.; Abi, B.; Abolins, M. et. al. *J. High Energy Phys.* **2013**, *07*, 032.

[4] Aad, G.; Abbott, B.; Abdallah, J.; Abdelalim, A. A.; Abdesselam, A.; Abdinov, O.; Abi, B.; Abolins, M.; Abramowicz, H.; Abreu, H. et al. *Phys. Rev. D* **2012**, *85*, 032009.

[5] Chatrchyan, S.; Khachatryan, V.; Sirunyan, A. M.; Tumasyan, A.; Adam, W.; Bergauer, D.; Dragicevic, M.; Erö, J.; Fabjan, C.; Friedl, M. et al. *J. High Energy Phys.* **2012**, *01*, 010.

[6] Khachatryan, V.; Sirunyan, A. M.; Tumasyan, A.; Adam, W.; Bergauer, T.; Dragicevic, M.; Erö, J.; Fabjan, C.; Friedl, M.; Fruehwirth, R. et al. *Phys. Rev. D* **2015**, *91*, 052008.

[7] Khachatryan, V.; Sirunyan, A. M.; Tumasyan, A.; Adam, W.; Bergauer, T.; Dragicevic, M.; Erö, J.; Fabjan, C.; Friedl, M.; Fruehwirth, R. et al. *J. High Energy Phys.* **2015**, *10*, 128.

[8] Khachatryan, V.; Sirunyan, A. M.; Tumasyan, A.; Adam, W.; Aşılar, E.; Bergauer, T.; Brandstetter, J.; Brondolin, E.; Dragicevic, M.; M.; Erö, J. et al. *J. High Energy Phys.* **2017**, *04*, 022.

[9] Aaij, R.; Beteta, C. A.; Adeva, B.; Adinolfi, M.; Ajaltouni, Z.; Akar, S.; Albrecht, J.; Alessio, F.; Alexander, M.; Ali, S. et al. *J. High Energy Phys.* **2016**, *05*, 131.

[10] Aaboud, M.; Aad, G.; Abbott, B.; Abdallah, J.; Abdinov, O.; Abeloos, B.; Aben, R.; AbouZeid, O.; Abraham, N.; Abramowicz, H. et al. *Eur. Phys. J. C* **2017**, *77*, 361.

[11] Sirunyan, A. M.; Tumasyan, A.; Adam, W.; Ambrogi, F.; Asilar, E.; Bergauer, T.; Brandstetter, J.; Brondolin, B.; Dragicevic, M.; Erö, J. et al. *Eur. Phys. J. C* **2017**, *78*, 965.

[12] Boughezal, R.; Campbell, J. M.; Ellis, R. K.; Focke, C.; Giele, W. T.; Liu, X.; Petriello, F. *Phys. Rev. Lett.* **2016**, *116*, 152001.

[13] Gehrmann-De Ridder, A.; Gehrmann, T.; Glover, E. W. N.; Huss, A.; Morgan, T. A. *J. High Energy Phys.* **2016**, *11*, 094.

[14] Gavin, R.; Li, Y.; Petriello, F.; Quackenbush, S. *Commun. Comput. Phys.* **2013**, *184*, 208-214.

[15] Catani, S.; Cieri, L.; Ferrera, G.; de Florian, D.; Grazzini, M. *Phys. Rev. Lett.* **2009**, *103*, 082001.

[16] Grazzini, M.; Kallweit, S.; Wiesemann, M. *Eur. Phys. J. C* **2018**, *78*, 537.

[17] Catani, S.; Grazzini, M. *Phys. Rev. Lett.* **2007**, *98*, 222002.

[18] Catani, S.; Cieri, L.; de Florian, D.; Ferrera, G.; Grazzini, M. *Eur. Phys. J. C* **2012**, *72*, 2195.

[19] Kosower, D. A. *Phys. Rev. D* **1998**, *57*, 5410-5416.

[20] Gehrmann-De Ridder, A.; Gehrmann, T.; Glover, E. W. N. *J. High Energy Phys.* **2005**, *09*, 056.

[21] Somogyi, G.; Trocsanyi, Z.; Del Duca, V. *J. High Energy Phys.* **2005**, *06*, 024.

[22] Boughezal, R.; Liu, X.; Petriello, F. *Phys. Rev. D* **2015**, *91*, 094035.

[23] Cacciari, M.; Dreyer, F. A.; Karlberg, A.; Salam, G. P.; Zanderighi, G. *Phys. Rev. Lett.* **2015**, *115*, 082002.

[24] Cascioli, F.; Maierhofer, P.; Pozzorini, S. *Phys. Rev. Lett.* **2012**, *108*, 111601.

[25] Buccioni, F.; Pozzorini, S.; Zoller, M. *Eur. Phys. J. C* **2018**, *78*, 70.

[26] Denner, A.; Dittmaier, S.; Hofer, L. *Commun. Comput. Phys.* **2017**, *212*, 220-238.

[27] Collins, J. C.; Soper, D. E.; Sterman, G. F. *Nucl. Phys. B* **1985**, *250*, 199-224.

[28] Bozzi, G.; Catani, S.; de Florian, D.; Grazzini, M. *Nucl. Phys. B* **2006**, *737*, 73-120.

[29] Buckly, A.; Ferrando, J.; Lloyd, S.; Nordström, K.; Page, B.; Rüfenacht, M.; Schönherr, M.; Watt, G. *Eur. Phys. J. C* **2015**, *75*, 132.

[30] Ball, R. D.; Bertone, V.; Carrazza, S.; Deans, C. S.; Debbio, L. D.; Forte, S.; Guffanti, A.; Hartland, N. P.; Latorre, J. I.; Rojo, J. et al. *J. High Energy Phys.* **2015**, *04*, 040.

[31] Cacciari, M.; Salam, G. P.; Soyez, G. *J. High Energy Phys.* **2008**, *04*, 063.

[32] Malik, S. A.; Watt, G. *J. High Energy Phys.* **2014**, *02*, 025.